been digested to completion with Bam HI; these libraries were screened with a probe corresponding to sequences within the transgene. The wild-type clones (D'3 and E'4) corresponding to the transgene insertion site were cloned by screening of a wild-type FVB/N partial Sau 3A–digested genomic lambda library with HRA, an internal Eco RI fragment from pλA6-7.6 that contains sequences flanking the transgene insertion. Total RNA was isolated by use of the guanidinium isothiocyanate procedure (*28*) and enriched for polyadenylated [poly(A)$^+$] RNA by passage through oligo(dT) columns. The cDNA library was prepared from poly(A)$^+$ RNA isolated from whole 14.5 days post-coitum (dpc) mouse embryos; Sma I adaptors and Eco RI ends were added and the double-stranded cDNAs ligated into the λgt10 vector (Stratagene). Hybridization probes were labeled with [α-^{32}P]deoxycytidine 5′-triphosphate (dCTP) by the random-hexamer labeling method (*29*). The Sanger dideoxynucleotide method was used for all sequencing (*30*).

22. J. H. Moyer *et al.*, unpublished results.
23. W. McGinnis, C. P. Hart, W. J. Gehring, F. H. Ruddle, *Cell* **38**, 675 (1984).
24. R. S. Sikorski, M. S. Boguski, M. Goebl, P. Hieter, *ibid.* **60**, 307 (1990).
25. M. Goebl and M. Yanagida, *Trends Biochem. Sci.* **16**, 173 (1991); I. Van der Leij, M. M. Franse, Y. Elgersma, B. Distel, H. F. Tabak, *Proc. Natl. Acad. Sci. U.S.A.* **90**, 11782 (1993).
26. R. P. Woychik *et al.*, *Proc. Natl. Acad. Sci. U.S.A.* **87**, 2588 (1990).
27. J. J. Schrick *et al.*, unpublished results.
28. J. Sambrook, E. F. Fritsch, T. Maniatis, in *Molecular Cloning: A Laboratory Manual* (Cold Spring Harbor Laboratory, Cold Spring Harbor, NY, ed. 2, 1989); F. M. Ausubel *et al.*, in *Current Protocols in Molecular Biology* (Wiley, New York, 1988).
29. A. P. Feinberg and B. Vogelstein, *Anal. Biochem.* **137**, 266 (1984).
30. F. Sanger, S. Nicklen, A. R. Coulson, *Proc. Natl. Acad. Sci. U.S.A.* **74**, 5463 (1977).
31. M. Kozak, *J. Cell Biol.* **115**, 887 (1991).
32. L. Stubbs *et al.*, *Genomics* **6**, 645 (1990).
33. We gratefully acknowledge E. Bohnlein for providing the pPyF9-1 construct, B. Beatty for generating the *TgN737Rpw* line by pronuclear microinjection, P. D'Eustachio for the mouse × Chinese hamster somatic cell hybrid DNAs, J. Nadeau for the *Rb-1* probe and the *Tcrα* cDNA that were used as probes in the interspecific backcross mapping analysis, B. L. Hogan and M. E. Dickinson for the *Rb-1* interspecies backcross hybridization experiment and interspecies backcross DNAs and panels, L. Stubbs for the 14.5-dpc cDNA library, and J. Bernstein and J. Rutledge for slides of human tissues. We also thank S. T. Reeders and L. F. Onuchic for their contribution in the computer analysis of the cDNA sequence, and E. M. Rinchik, R. J. Mural, W. R. Jacobs, J. H. Nadeau, and B. L. M. Hogan for critically reading the manuscript. Supported by the Office of Health and Environmental Research, U.S. Department of Energy under contract DE-AC05-84OR21400 with Martin Marietta Energy Systems, Inc. (R.P.W.), the National Institute of Environmental Health Sciences under contract IAG 222Y01-ES-10067 (R.P.W., M.J.L.-T., and H.-Y.K.), National Institute of Diabetes and Digestive and Kidney Diseases grant 1 R01 DK45633-01 (J.E.W. and R.P.W.), National Institute of Child Health and Human Development grant R01 HD25323 (R.P.W.), and by NIH predoctoral National Research Service Award NR06789-01 from the National Center for Nursing Research (J.H.M.). Additional support was provided by NIH grant 5 R01 DK44875 (E.D.A. and W.E.S.). All mice used in this study were handled in accordance with the NIH Guide for the Care and Use of Laboratory Animals.

23 December 1993; accepted 7 April 1994

Summation and Division by Neurons in Primate Visual Cortex

Matteo Carandini and David J. Heeger

Recordings from monkey primary visual cortex (V1) were used to test a model for the visually driven responses of simple cells. According to the model, simple cells compute a linear sum of the responses of lateral geniculate nucleus (LGN) neurons. In addition, each simple cell's linear response is divided by the pooled activity of a large number of other simple cells. The cell membrane performs both operations; synaptic currents are summed and then divided by the total membrane conductance. Current and conductance are decoupled (by a complementary arrangement of excitation and inhibition) so that current depends only on the LGN inputs and conductance depends only on the cortical inputs. Closed form expressions were derived for fitting and interpreting physiological data. The model accurately predicted responses to drifting grating stimuli of various contrasts, orientations, and spatiotemporal frequencies.

Since the pioneering work of Hubel and Wiesel (*1*), there have been a multitude of physiological experiments that studied the visually driven responses of V1 simple cells. A long-standing view is that a simple cell's response depends on a linear sum, over local space and recently past time, of the intensity values in the stimulus (*2*). The linear model of simple cell physiology is attractive because the response of a linear cell can be completely characterized with a relatively small number of measurements. In addition, the linear model explains the selectivity of simple cells for stimulus position, orientation, and direction of motion.

Unfortunately, the linear model falls short of a complete account of simple cell physiology. According to the linear model, doubling the contrast of a (periodic) drifting grating stimulus would double the response so one would record twice as many action potentials during each period of stimulation. However, simple cells do not behave this way. First, response amplitude saturates at high contrasts (*3*); doubling the contrast yields fewer than twice the number of action potentials. Second, response phase advances with contrast (*4*); when contrast is doubled, the action potentials occur sooner during each period of stimulation.

A third fault with the linear model in regard to simple cells is revealed by tests of superposition. A typical simple cell responds vigorously to its preferred orientation but not at all to a perpendicular orientation. According to the linear model, the response to the superimposed pair of stimuli (preferred plus perpendicular) should equal the response to the preferred stimulus presented alone. In fact, the response to the superimposed pair is about half that predicted (*5*), a phenomenon known as cross-orientation inhibition.

To explain these nonlinear aspects of simple cell responses, we have recently proposed a new model of simple cell responses, called the normalization model (*6*). This model (Fig. 1) begins with an underlying linear stage. The linear stage is followed by a normalization stage, where each cell's linear response to the stimulus is divided by a quantity proportional to the pooled activity of a large number of other cells. Normalization is a nonlinear operation; one input (a cell's underlying linear response) is divided by another input (the pooled activity of a large number of cells). The effect of normalization is that the response of each cell is rescaled with respect to stimulus contrast.

The normalization model explains a large body of otherwise unexplained physiological phenomena (*6*). According to the model, a cell's selectivity is attributed to summation (the linear stage) and its nonlinear behavior is attributed to division (the normalization stage). The model explains response amplitude saturation because the divisive suppression increases with stimulus contrast. The model also explains cross-orientation inhibition because a given cell is suppressed by many other cells, including those with perpendicular orientation tunings. Until now, however, two problems still remained to be solved. First, there was no explanation for why response phase depends on contrast. Second, there was no explanation for how the summation and division computations might be implemented by cortical neurons.

It is common to characterize the electrical behavior of a cell's membrane with electrical circuits made up of resistors and capacitors (Fig. 2). The input to a cell is a current driven by the synaptic conduc-

M. Carandini, Center for Neural Science, New York University, New York, NY 10003, USA.
D. J. Heeger, Department of Psychology, Stanford University, Stanford, CA 94305, USA.

tances that vary over time depending on the firing rates of the presynaptic cells. The membrane potential changes over time, given the present value of the membrane potential and the present synaptic conductances

$$-C\frac{dV}{dt} = g_i(V - V_i) + g_e(V - V_e) + g_{shunt}(V - V_{shunt} + g_{leak}(V - V_{leak}) \quad (1)$$
$$= gV - I_d$$

where

$$I_d = g_eV_e + g_iV_i + g_{shunt}V_{shunt} + g_{leak}V_{leak}$$
$$g = g_e + g_i + g_{shunt} + g_{leak}$$

and where C is the membrane capacitance, V_e, V_i, and V_{shunt} are excitatory, inhibitory, and shunt equilibrium potentials, respectively, g_e, g_i, and g_{shunt} are the variable conductance resistors, and g_{leak} and V_{leak} determine the leak current. We define I_d to be the cell's driving current; it has the units of current and depends on the cell's synaptic inputs but is independent of the cell's membrane potential V. The driving current can be measured by voltage-clamping the cell at $V = 0$.

Solving Eq. 1 yields an expression for the cell's membrane potential as a function of the synaptic conductances (*7*)

$$V = \left[\theta \frac{g}{C} \exp\left(\frac{-tg}{C}\right)\right] * \left[\frac{I_d}{g}\right] \quad (2)$$

where $\theta = 1$ if time $t > 0$ and $\theta = 0$ otherwise. Equation 2 is a typical textbook formulation of the synaptic input to a neuron. The membrane potential V is equal to the driving current, I_d, divided by the total conductance, g, and then convolved with an exponential low-pass filter. The relation between the membrane potential and the instantaneous firing rate, R, can be approximated (*8*) by half-wave rectification followed by squaring

$$R \propto [\max(0, V - V_{rest})]^2 \quad (3)$$

where V_{rest} is the membrane potential in the absence of visual stimulation.

To develop a biophysical mechanism that performs both summation and division, we postulate that there are two sets of inputs: the "linear" synaptic conductances and the "normalization" synaptic conductances. The linear synapses regulate g_e and g_i and are contributed by neurons in the lateral geniculate nucleus (LGN). The normalization synapses regulate g_{shunt} and are contributed by all the cortical neurons in the normalization pool. In addition, we postulate that the equilibrium potential of the normalization synapses, V_{shunt}, is equal to a cell's resting potential (*9*). For simplicity of notation, we chose $V_{rest} = V_{shunt} = 0$ and specified all other voltages with respect to this origin. Finally, we postulate that the linear inputs trade off against one another:

$$g_i + g_e + g_{leak} = g_0 \quad (4)$$

where g_{leak} and g_0 are constants. When there is no visual stimulation, the cell's conductance equals g_0, partly a result of the spontaneous activity of the presynaptic cells and partly because the membrane has nonzero conductance. Equation 4 is the key property of our model because it allows us to decouple current from conductance. Changes in the cell's total conductance, g, depend only on the normalization inputs (because g_0 is a constant), and changes in the driving current, I_d, depend only on the linear inputs (because $V_{shunt} = 0$). One could implement Eq. 4 by having a complementary arrangement of inputs: g_e could be driven by on-center LGN cells and g_i by off-center LGN cells with spatially superimposed receptive fields (Fig. 1). In this way, an increase in the excitatory conductance from the LGN would be matched by a decrease in the inhibitory conductance and vice versa (*10*).

Our model achieves normalization because a cell's conductance depends on the total activity of all the cells in the normalization pool. Changing the conductance, g, has two effects on the membrane potential: (i) It changes the gain (sensitivity to input) because the cell's driving current is scaled by conductance and (ii) it changes the dynamics because the cell's time constant (C/g) is also scaled by conductance (Eq. 2).

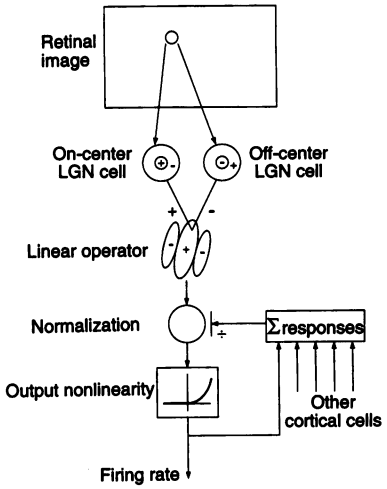

Fig. 1. Illustration of the normalization model. A linear stage combines complementary inputs from the LGN. The central excitatory subregion of the receptive field sums responses of on-center cells and subtracts responses of off-center cells with spatially superimposed receptive fields (*10*). The flanking inhibitory subregions are obtained by the opposite arrangement of excitation and inhibition. A normalization stage divides the linear stage's response by the pooled activity of a large number of cortical cells. Finally, the response of the normalization stage is half-wave–rectified and squared (*8*).

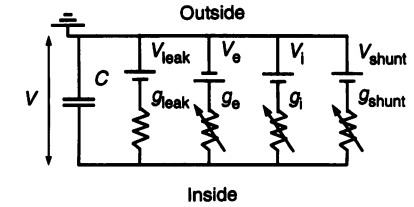

Fig. 2. Equivalent circuit model of a cellular membrane. The capacitor represents the capacitance, C, of the membrane. The equilibrium potentials (V_e, V_i, and V_{shunt}) of synaptic ion channels are represented by batteries. The number of open synaptic ion channels is represented by variable conductance resistors (g_e, g_i, and g_{shunt}). The leak current is determined by a resistor (g_{leak}) and a battery (V_{leak}).

To test the model, we recorded the responses of simple cells in anesthetized paralyzed macaque monkeys (*11*) while presenting drifting sinusoidal grating stimuli of various contrasts, orientations, and spatiotemporal frequencies. We used the normalization model to fit the amplitude and phase of the first harmonic of the responses. According to the model, increasing stimulus contrast should yield an increase in membrane conductance that, in turn, should yield a decrease in gain (response amplitude saturation) and a decrease in the time constant (response phase advance).

Results for a typical cell are shown in Fig. 3; similar results were obtained for nine other cells. As predicted by the model, response amplitude saturates and response phase advances with increasing contrast. By comparison, the response phase of a linear cell would be constant and the response amplitude of a linear cell would not saturate.

Our model explains another important aspect of the responses: Amplitude saturation and phase advance do not depend on stimulus orientation. In Fig. 3E, the two response amplitude curves (for preferred and nonpreferred orientations) are vertically shifted copies of one another; because the data are plotted on a logarithmic response scale, this means that the ratio of response amplitudes is about the same at all stimulus contrasts. Likewise, in Fig. 3F, the difference in response phases does not depend on contrast. These invariances, which we attribute to normalization, are critical for encoding information about orientation independent of contrast. Similar vertical shifts of log response amplitude versus contrast have been reported for stimuli of nonpreferred spatial frequency and direction of motion (*3*, *12*). The vertical shift of response phase has not been reported previously.

For 7 of our 10 cells, we measured responses at different temporal frequencies

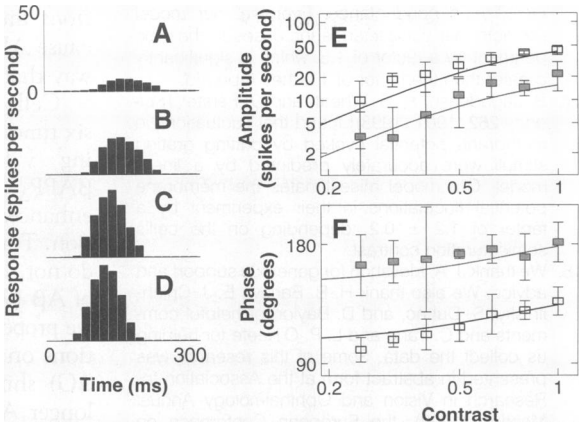

Fig. 3. (**A** through **D**) One cycle of the response of a V1 simple cell to drifting sinusoidal gratings of contrast 0.125, 0.25, 0.5, and 1.0, respectively; temporal frequency was 3 Hz. The response amplitude saturation is evident because stimulus contrast doubles from (C) to (D), but height does not double. The response phase advance is evident because the peak in (D) is almost 50 ms earlier than that in (A). (**E** and **F**) Amplitude and phase of the fundamental Fourier component of the response of a V1 simple cell to drifting sinusoidal gratings that varied in contrast and orientation. This cell was tested with 90 randomly interleaved stimuli (three temporal frequencies, three orientations, and 10 contrasts). Here we show only the responses for one temporal frequency (6 Hz) and for two orientations: preferred orientation (open symbols) and 20° from the preferred orientation (filled symbols). Error bars represent ±1 SD (n = 5). The continuous curves in each plot show the best fit of our model. The model is mathematically tractable, enabling us to derive closed form expressions for fitting and interpreting physiological data. Response amplitude as a function of stimulus contrast c and stimulus temporal frequency ω is given by

$$\text{amplitude}(R) = K\frac{c^2}{g^2 + (\omega C)^2}$$

where C is capacitance, $g = \sqrt{g_0^2 + k^2c^2}$ (conductance), and g_0, K, and k are constants. Response phase is given by phase(R) = ϕ + arctan(ωC/g) where ϕ is another constant. The free parameters of the fit are the response gain and phase (K and ϕ, different for each orientation and temporal frequency) of the underlying linear stage, the time constant of the membrane at rest (C/g_0), and the strength of the normalization signal (k/g_0).

and used the model to estimate the time constant of the membrane (that is, membrane capacitance divided by membrane conductance). The estimated time constant at rest (zero contrast) varied in our cells from 0 to 98.5 ms (mean = 27.8 ms). These values are consistent with published intracellular measurements (*13*). The estimated membrane time constant decreased on average by a factor of 3.7 ± 0.7, when contrast was increased from 0 to 1. In other words, we predict that the conductance of a simple cell should increase about fourfold when the cell is presented with a full contrast grating and that this conductance increase should be independent of stimulus orientation (*14*, *15*).

Simple cells have a limited dynamic range, a limit to how strong an output signal they can generate and, hence, a limit to the range of contrasts over which they can respond differentially. Normalization makes it possible for response ratios to be independent of stimulus contrast (shown by the vertical shift of the curves in Fig. 3E), even in the face of response saturation. This invariance is critical for encoding visual information (about motion, orientation, binocular disparity, and other factors) independent of contrast. Normalization thus preserves the essential features of linearity in a system, that of the brain, that has limited dynamic range.

Although there is direct empirical support for the complementary arrangement of the linear summation inputs in our model (*10*), our mechanism for division is not consistent with recent intracellular measurements that show (i) slight conductance increases (*16*) and (ii) no indication that membrane potential is normalized (*17*). We could reconcile our model with these intracellular results by proposing a variation of the model that yields the same (firing rate) responses without corresponding conductance increases. This second model still has a complementary arrangement of inputs to perform linear summation, but it uses a different mechanism for division. We have been assuming that the transformation between membrane potential and firing rate is not affected by the visual stimulus and that division is implemented by changing conductance. Instead, division might be implemented by changing the gain of the firing mechanism. Further intracellular measurements could clearly distinguish between these two possibilities.

REFERENCES AND NOTES

1. D. Hubel and T. Wiesel, *J. Physiol.* (*London*) **160**, 106 (1962).
2. F. W. Campbell, G. F. Cooper, C. Enroth-Cugell, *ibid.* **203**, 223 (1969); J. A. Movshon, I. D. Thompson, D. J. Tolhurst, *ibid.* **283**, 53 (1978).
3. D. G. Albrecht and D. B. Hamilton, *J. Neurophysiol.* **48**, 217 (1982).
4. A. F. Dean and D. J. Tolhurst, *Exp. Brain Res.* **62**, 143 (1986).
5. A. B. Bonds, *Visual Neurosci.* **2**, 41 (1989).
6. D. J. Heeger, *ibid.* **9**, 181 (1992); *ibid.*, p. 427; *J. Neurophysiol.* **70**, 1885 (1993). For related models, see G. Sperling and M. M. Sondhi, *J. Opt. Soc. Am.* **58**, 1133 (1968); S. Grossberg, *Neural Networks* **1**, 17 (1988); D. G. Albrecht and W. S. Geisler, *Visual Neurosci.* **7**, 531 (1991).
7. This solution is exact when the total conductance is constant over time. It is an approximate solution when the total conductance varies slowly over time. For simplicity, we dropped the term that corresponds to the initial condition.
8. Firing rate is proportional to membrane depolarization, once above threshold [C. E. Stafsrom, P. C. Schwindt, W. E. Crill, *J. Neurophysiol.* **52**, 264 (1984)]. To simplify the mathematics, we approximate the threshold by half-wave rectification and squaring

$$\max(0, V - V_{\text{thresh}}) \approx m[\max(0, V - V_{\text{rest}})]^2$$

where m is a constant and V_{thresh} is the spike threshold. This approximation is reasonable because (i) $V_{\text{rest}} < V_{\text{thresh}}$ (simple cells typically have no spontaneous activity) and (ii) the relevant range of membrane potentials is limited.
9. Shunting inhibition is a widely cited proposal for how neurons might perform division [J. S. Coombs, J. C. Eccles, P. Fatt, *J. Physiol.* (*London*) **130**, 396 (1955); C. Koch and T. Poggio, in *Synaptic Function*, G. M. Edelman, W. E. Gall, W. M. Cowan, Eds. (Wiley, New York, 1987), pp. 637–698]. Because the equilibrium potential for chloride, V_{Cl}, is close to a cell's resting potential, opening chloride channels will change the cell's conductance without introducing much current. Chloride shunting, however, only approximates division because V_{Cl} is not exactly equal to V_{rest}. Exact division can be implemented with two synaptic conductances, one excitatory and one inhibitory, that increase (or decrease) in proportion such that

$$g_i'V_i + g_e'V_e = I_0$$

where I_0 is a constant current (note that V_e and V_i have opposite sign). This pair of channels has an effective equilibrium potential

$$V_{\text{shunt}} = \frac{I_0}{g_e' + g_i'}$$

and a conductance

$$g_{\text{shunt}} = g_e' + g_i'$$
10. There is evidence for complementary excitation and inhibition as expressed by Eq. 4 [P. Heggelund, *Exp. Brain Res.* **42**, 89 (1981); L. A. Palmer and T. L. Davis, *J. Neurophysiol.* **46**, 260 (1981); D. Ferster, *J. Neurosci.* **8**, 1172 (1988); _____ and B. Jagadeesh, *ibid.* **12**, 1262 (1992); R. J. Douglas, K. A. C. Martin, D. Whitteridge, *J. Physiol.* (*London*) **440**, 659 (1991)]. There is, however, no evidence for direct thalamocortical inhibition, so the inhibition most likely comes indirectly through other cortical cells.
11. Together with J. A. Movshon, L. P. O'Keefe, and C. Tang, we recorded the extracellular activity of cells in the primary visual cortices of three paralyzed and anesthetized macaque monkeys. Our results are from 10 cells that were chosen out of 106 for the following reasons: (i) they were readily classified as simple cells; (ii) they were tested at least twice; and (iii) they showed satisfactory stability and isolation for the duration of the test (>1 hour). All cells were tested with a variety of contrasts and orientations (or spatial frequencies). Seven of the 10 were also tested with different temporal frequencies.
12. C. Li and O. Creutzfeldt, *Pflugers Arch.* **401**, 304 (1984).
13. C. E. Stafsrom, P. C. Schwindt, W. E. Crill, *J. Neurophysiol.* **52**, 278 (1984); T. Ogawa, *Brain Res.* **226**, 315 (1981); K. Stratford *et al.*, in *The Computing Neuron*, R. Durbin *et al.*, Eds. (Addison-Wesley, New York, 1990), pp. 296–321.
14. A fourfold increase in conductance is not inconceivable; computer simulations of a pyramidal cell [Ö. Bernander, R. J. Douglas, K. A. C. Martin, C.

Koch, *Proc. Natl. Acad. Sci. U.S.A.* **88**, 11569 (1991)] have indicated that membrane conductance can increase by a factor of 10.
15. The main (parvocellular) input to the monkey cortex is remarkably linear, exhibiting neither response amplitude saturation nor response phase advance. Magnocellular inputs in the monkey, however, show both strong amplitude saturation and prominent response phase advance [R. M. Shapley, *Annu. Rev. Psychol.* **41**, 635 (1990); E. A. Benardete, E. Kaplan, B. W. Knight, *Visual Neurosci.* **8**, 483 (1992)]. Our prediction of a fourfold increase in conductance is based on the assumption that inputs from the LGN are themselves linear. If simple cells receive significant magnocellular input this assumption is wrong, and we are overestimating the dependence of conductance on stimulus contrast.
16. N. J. Berman, R. J. Douglas, K. A. C. Martin, and D. Whitteridge [*J. Physiol. (London)* **440**, 697 (1991)] measured only slight conductance increases for a drifting bar stimulus. However, a drifting bar is a weak stimulus; stimulus energy is formally defined as the integral of the power spectrum (the Fourier energy) of the stimulus. Our model predicts that a stronger stimulus (like a full contrast drifting grating) would yield a larger increase in conductance. Even so, our model predicts that conductance increases in their experiment by a factor of 1.5, which is significantly greater than the factor of 1.2 they reported.
17. B. Jagadeesh, H. S. Wheat, and D. Ferster [*Science* **262**, 1901 (1993)] found that fluctuations in membrane potential evoked by drifting grating stimuli were accurately predicted by a linear model. Our model misestimates the membrane potential fluctuations in their experiment by a factor of 1.2 ± 0.2, depending on the cell's semisaturation contrast.
18. We thank J. A. Movshon for generous support and advice. We also thank H. B. Barlow, E. J. Chichilnisky, S. DuLac, and D. Baylor for helpful comments and C. Tang and L. P. O'Keefe for helping us collect the data. Some of this research was presented in abstract form at the Association for Research in Vision and Ophthalmology Annual Meeting (1993), the European Conference on Visual Perception (1993), and the Society for Neuroscience Annual Meeting (1993). Supported by Consiglio Nazionale delle Ricerche (Italy), by National Institute of Mental Health grant 1-R29-MH50228-01, and by NASA grant NCC2-307.

8 December 1993; accepted 19 April 1994

An Increased Percentage of Long Amyloid β Protein Secreted by Familial Amyloid β Protein Precursor (βAPP_{717}) Mutants

Nobuhiro Suzuki,* Tobun T. Cheung,* Xiao-Dan Cai, Asano Odaka, Laszlo Otvos Jr., Christopher Eckman, Todd E. Golde, Steven G. Younkin†

Normal processing of the amyloid β protein precursor (βAPP) results in secretion of a soluble 4-kilodalton protein essentially identical to the amyloid β protein (Aβ) that forms insoluble fibrillar deposits in Alzheimer's disease. Human neuroblastoma (M17) cells transfected with constructs expressing wild-type βAPP or the βAPP_{717} mutants linked to familial Alzheimer's disease were compared by (i) isolation of metabolically labeled 4-kilodalton Aβ from conditioned medium, digestion with cyanogen bromide, and analysis of the carboxyl-terminal peptides released, or (ii) analysis of the Aβ in conditioned medium with sandwich enzyme-linked immunosorbent assays that discriminate $A\beta_{1-40}$ from the longer $A\beta_{1-42}$. Both methods demonstrated that the 4-kilodalton Aβ released from wild-type βAPP is primarily but not exclusively $A\beta_{1-40}$. The βAPP_{717} mutations, which are located three residues carboxyl to $A\beta_{43}$, consistently caused a 1.5- to 1.9-fold increase in the percentage of longer Aβ generated. Long Aβ (for example, $A\beta_{1-42}$) forms insoluble amyloid fibrils more rapidly than $A\beta_{1-40}$. Thus, the βAPP_{717} mutants may cause Alzheimer's disease because they secrete increased amounts of long Aβ, thereby fostering amyloid deposition.

The 39– to 43–amino acid polypeptide Aβ, deposited as amyloid (*1*, *2*) in the brains of patients with Alzheimer's disease (AD), is derived from a set of 677 to 770 amino acid proteins collectively referred to as βAPP (*2*–*4*). Strong evidence that amyloid deposition plays a critical role in the development of AD has come from the identification of familial AD (FAD) kindreds in which the AD phenotype cosegregates with mutations in the βAPP gene. Three of the FAD-linked βAPP mutations convert the valine located three residues carboxyl to $A\beta_{43}$ (Val^{717} in βAPP_{770}) to isoleucine (ΔI) (*5*), phenylalanine (ΔF) (*6*), or glycine (ΔG) (*7*). A fourth double mutation (ΔNL) alters the lysine-methionine located immediately amino to $A\beta_1$ (Lys^{670}-Met^{671} in βAPP_{770}) to asparagine-leucine (*8*). The location of these mutations immediately suggests that they may cause AD by altering βAPP processing in a way that is amyloidogenic.

Cells expressing $\beta APP_{\Delta NL}$ secrete five to six times more 4-kD Aβ than those expressing wild-type βAPP (*9*, *10*). Thus, $\beta APP_{\Delta NL}$ undergoes altered processing that enhances the likelihood of amyloid deposition. Transfected cells expressing $\beta APP_{695\Delta I}$ do not, however, release increased amounts of Aβ (*9*). To account for this observation, we proposed (*9*) that the FAD-linked mutations on the carboxyl side of Aβ (ΔI, ΔF, ΔG) shift cleavage to favor generation of longer Aβs such as $A\beta_{1-42}$ or $A\beta_{1-43}$. Because these longer Aβs form amyloid fibrils more rapidly than $A\beta_{1-40}$ (*11*, *12*), shifting the site of cleavage could result in amyloid deposition without increasing the overall amount of Aβ produced. Here we have used two different methods to test this hypothesis.

Our initial approach was to label transfected M17 cells with [^{35}S]methionine plus either [^{3}H]valine or [^{3}H]isoleucine. The radioactively labeled Aβ in conditioned medium was then separated by immunoprecipitation and tris-tricine SDS–polyacrylamide gel electrophoresis (PAGE) as previously described (*13*), transferred to immobilon, visualized autoradiographically, and excised. The excised 4-kD Aβ was digested with cyanogen bromide (CNBr), which cleaves Aβ on the carboxyl side of the methionine at $A\beta_{35}$, releasing COOH-terminal peptides beginning at $A\beta_{36}$ (for example, $A\beta_{36-40}$ from $A\beta_{1-40}$, $A\beta_{36-42}$ from $A\beta_{1-42}$). Finally, the radiolabeled CNBr peptides were separated by reversed-phase liquid chromatography (RPLC) with a Vydac narrow bore C4 column. CNBr digestion was carried out in the presence of excess unlabeled $A\beta_{36-40}$ and $A\beta_{36-42}$ both to improve recovery of the labeled COOH-terminal peptides and to mark, by ultraviolet absorbance, the fractions in which $A\beta_{36-40}$ and $A\beta_{36-42}$ elute.

The radioactively labeled COOH-terminal peptides that CNBr releases from the 4-kD Aβ produced by M17-βAPP_{695} cells labeled with [^{35}S]methionine plus [^{3}H]valine are shown in Fig. 1A. The major radiolabeled peptide eluted from the C4 column with unlabeled $A\beta_{36-40}$. In addition, there was minor labeled peptide that eluted with unlabeled $A\beta_{36-42}$ (*14*). To further characterize these COOH-terminal peptides, we examined the large amount of 4-kD Aβ released from M17-$\beta APP_{695\Delta NL}$ cells labeled with [^{35}S]methionine plus either [^{3}H]valine or [^{3}H]isoleucine (Fig. 1B). We identified the major COOH-terminal peptide released from this 4-kD Aβ by CNBr digestion as $A\beta_{36-40}$ by (i) radiosequencing it to show valine residues at positions 1 and 4 as expected (*15*), (ii) demonstrating (Fig. 1B) that it is not labeled by [^{3}H]isoleucine and therefore terminates be-

N. Suzuki and A. Odaka, Discovery Research Division, Takeda Chemical Industries, Ltd., Wadai 10, Tsukuba, Ibaraki, 300-42 Japan.
T. T. Cheung, X.-D. Cai, C. Eckman, T. E. Golde, S. G. Younkin, Division of Neuropathology, Institute of Pathology, Case Western Reserve University, Cleveland, OH 44106, USA.
L. Otvos Jr., The Wistar Institute of Anatomy and Biology, Philadelphia, PA 19104, USA.
*These authors contributed equally to this study.
†To whom correspondence should be addressed.

Summation and Division by Neurons in Primate Visual Cortex

Matteo Carandini, and David J. Heeger

Science, 264 (5163), • DOI: 10.1126/science.8191289